31st Annual International Conference of the IEEE EMBS
Minneapolis, Minnesota, USA, September 2-6, 2009

A Numerical Model to study Auscultation Sounds under Pneumothorax conditions

Sridhar Ramakrishnan, *Student Member, IEEE,* Satish Udpa, *Fellow, IEEE,* and Lalita Udpa, *Fellow, IEEE*

***Abstract*—A 2D viscoelastic finite-difference time-domain (FDTD) is used to simulate sound propagation of lung sounds in the human thorax. Specifically, the model is employed to study the effects of pneumothorax on the sounds reaching the thoracic surface. By simulating varying degrees of severity of the disease, the model assists in determining the key frequency bands that contain the most information to aid in diagnosis. The work thus lends itself for development of advanced auscultatory techniques for detection of pneumothorax using noninvasive acoustic sensors.**

I. Introduction

PNEUMOTHORAX is a pathological condition of the lungs in which air collects in the pleural space, i.e. the space that surrounds the lungs, leading to a lung-collapse eventually. Since it is a potentially life threatening disease, and is easily treatable when diagnosed early, there is significant interest in developing a noninvasive, low-cost, quick and advanced diagnostic scheme. Currently, the gold-standard technique for diagnosis of pneumothorax is the chest X-ray or a chest CT although misdiagnosis rates of around 30% have been reported even with these methods [1], [2].

Auscultation sounds offer a viable alternative for the diagnosis of various thoracic pathologies including pneumothorax [3]. Prior experimental studies have shown the effectiveness of breath sounds in differentiating between normal and pneumothorax conditions. By digitizing these sounds using acoustic sensors mounted around the torso, and combined with an intelligent multi-sensor processing scheme, one could devise a low-cost, noninvasive and portable solution for accurate diagnosis that may be even used for out-patient home monitoring purposes.

Recent times have seen several array-processing and pattern recognition studies attempting to exploit the spatio-temporal distribution of chest sounds for characterizing different pathologies in patients with heart or lung diseases. Although there has been some success in these efforts, not many schemes account for the effects of heterogeneity of the medium, shear waves contributions and extreme near-field conditions in their algorithms. This compels one to develop an accurate sound propagation forward model that incorporates these complexities, which can thereby assist in the development of better array processing schemes.

In the past, there have been numerous acoustic models developed to gather a better understanding of the transmission of sounds in the human thoracic cavity [4, 5]; however a majority of these either assume a very simple geometry or ignore the shear wave effects. Reference [6] presents an interesting study of comparing signals obtained using a boundary-element numerical scheme and experimental observations for a pneumothoracic condition. However, the work does not take into account all the anatomical features of the thorax into its model. This paper employs an acoustic model described in [7] that uses a 2D finite-difference time-domain (FDTD) numerical scheme embodying the true geometry and elastic material properties of the various tissues structures in the human torso. The model thus facilitates the study of effects of pneumothorax on the acoustic sensor signals and can be used to develop and validate various multi-sensor processing algorithms for diagnostic purposes. It also allows one to develop newer inverse problem solutions to localize and quantify the size of the pneumothoracic air cavity in the thorax.

Section 2 provides details of the development of the viscoelastic 2D FDTD model for lung sound propagation in the human thorax. Simulations details pertaining to modeling the pneumothorax conditions using the FDTD codes are discussed in Section 3. Preliminary simulation results demonstrating the effect of varying sizes of air cavity on the source-to-sensor transfer functions are presented in Section 4. Concluding remarks discussing the future steps to be taken to address some of the unresolved issues are presented in Section 5.

II. FDTD Model of Thorax

Auscultation sounds contain most of their energy at the lower audible range of frequencies. At these frequencies, compression and shear wave propagation can be significant in many of the tissues of the thorax. In addition, the heterogeneity of the medium results in mode conversions at each interface, thereby resulting in complex acoustic paths from an intra-thoracic source to a sensor on the chest. Thus,

Manuscript received April 7, 2009.

Sridhar Ramakrishnan is with the Electrical Engineering Department, Michigan State University, East Lansing, MI 48823 USA (phone: 517-303-1335; fax: 517-353-1980; e-mail: rsridhar@egr.msu.edu).

Satish Udpa is with the Electrical Engineering Department, Michigan State University, East Lansing, MI 48823 USA (e-mail: udpa@egr.msu.edu).

Lalita Udpa is with the Electrical Engineering Department, Michigan State University, East Lansing, MI 48823 USA (e-mail: udpal@egr.msu.edu).

in order to have a reasonably accurate acoustic model of the human thorax, it is imperative to take into account both the bulk and shear modulus along with fairly good estimates of the geometries of the various anatomical structures in the thorax.

A. Thoracic Anatomy and Material Properties

A transverse cross sectional photographic slice at the mid-thorax level passing through the heart acquired from the United States National Library of Medicine's Visible Human Project, as shown in Fig. 1 was used as the 2D image for the numerical model [8]. Each of the major tissue structures and their respective boundaries were carefully identified, and the corresponding material properties, namely density, longitudinal and shear wave velocities, the Lamé constants and the viscoelasticity coefficients were assigned [7].

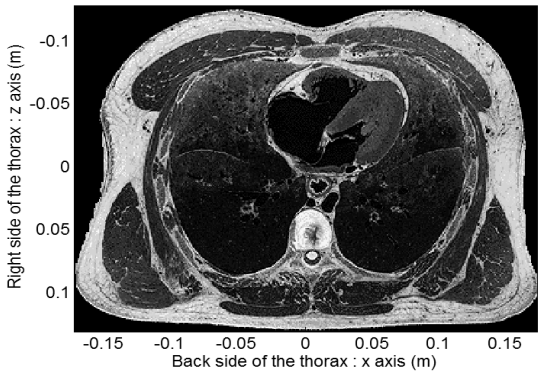

Fig. 1. Photographic cross-sectional slice of human thorax obtained from Visible Human Project

B. Governing Equations and Boundary Conditions

Wave propagation in a 2D viscoelastic medium is governed by the following momentum-conservation and constitutive equations:

$$\begin{aligned}
\rho\frac{\partial v_x}{\partial t} &= \frac{\partial T_{xx}}{\partial x}+\frac{\partial T_{xz}}{\partial z}+f_x\\
\rho\frac{\partial v_z}{\partial t} &= \frac{\partial T_{xz}}{\partial x}+\frac{\partial T_{zz}}{\partial z}+f_z\\
\frac{\partial T_{xx}}{\partial t}+\gamma_{xx}T_{xx} &= (\lambda+2\mu)\frac{\partial v_x}{\partial x}+(\lambda)\frac{\partial v_z}{\partial z}\\
\frac{\partial T_{zz}}{\partial t}+\gamma_{zz}T_{zz} &= (\lambda)\frac{\partial v_x}{\partial x}+(\lambda+2\mu)\frac{\partial v_z}{\partial z}\\
\frac{\partial T_{xz}}{\partial t}+\gamma_{xz}T_{xz} &= \mu\left(\frac{\partial v_x}{\partial z}+\frac{\partial v_z}{\partial x}\right)
\end{aligned} \tag{1}$$

where v_x, v_z are particle velocity components in the x and z directions respectively, T_{xx}, T_{zz} are the normal stress components in the x and z directions respectively and γ_{xx}, γ_{zz} are the corresponding resistance coefficients, T_{xz} is the shear stress component in the x-z plane and γ_{xz} is its corresponding resistance coefficient, f_x, f_z are the forcing functions in the x and z directions respectively, ρ is the density, and λ, μ are the Lamé constants. The viscoelasticity of the various tissues are incorporated as the resistance coefficients to the stress components.

Free-space boundary conditions are imposed by using a perfectly matched layer (PML) of air around the thoracic cavity. A theoretical reflection coefficient of 0.001 is used in the expressions of the loss factor in the PML region [9].

The material properties at interface regions between two layers are averaged to guarantee stability of the FDTD codes [10].

C. FDTD Implementation

A staggered grid leap-frog center-differencing scheme was used to discretize the equations in (1), which yield a second order accurate solution to the problem [11]. The PML boundary conditions are incorporated using a non-split complex frequency-shifted recursive integration technique [9].

The spatial grid size is determined based on the number of spatial sample points (K_s) chosen to track the shortest wavelength in the medium. Thus, if $c_{s,min}$ is the slowest shear wave to be traced and f_{max} is the bandwidth of the forcing function, then the grid size is obtained by

$$\Delta x = \Delta z = \frac{1}{K_s}\frac{c_{s,\min}}{f_{\max}} \tag{2}$$

The Courant condition governs the discretization in the time domain, according to which

$$\Delta t \le \frac{1}{\sqrt{2}}\frac{\Delta x}{c_{p,\max}} \tag{3}$$

must be satisfied in the entire spatial domain, where $c_{p,max}$ is the maximum longitudinal wave velocity in the medium.

D. Source Model

Modeling of the actual sources in the human thoracic cavity, namely the heart sources that include the opening and closing of the valves, haemodynamics in the valve chambers; the respiratory sources that include the vesicular, tracheal and bronchial sounds; and sources in the gastrointestinal tract is beyond the scope of this work. Since the primary focus of the work is on sound propagation characteristics, the source models employed here are somewhat simplistic in nature.

The simulations in the current work use a first derivative gaussian pulse as the f_z component of a point forcing function, with a center frequency f_0, located approximately at the point where the secondary bronchus meets the plane of the cross-sectional slice in the right lung. The source function is modeled as,

$$\begin{aligned}
f_z(t) &= B(t-t_S)\left[\frac{1}{\sqrt{2\pi}\sigma}e^{\frac{-(t-t_S)^2}{2\sigma^2}}\right] \quad \forall t \ge 0\\
&= 0, \quad \forall t < 0\\
f_x(t) &= 0, \quad \forall t\\
\sigma &= \frac{1}{2\pi f_0},\ B = \frac{Ae^{0.5}}{\sigma},\ t_S = 5\sigma
\end{aligned} \tag{4}$$

where B is defined such that a peak magnitude of A is established at the center frequency f_0.

E. Validation of FDTD Code

In order to validate the FDTD simulation codes, the results obtained are compared to analytical expressions derived for a homogeneous infinitely extending medium with a density of 1000 kg/m^3, and longitudinal and shear velocities of 1500 m/s and 500 m/s with a point force source acting at the origin. The first derivative of a gaussian pulse with a center frequency of 1 kHz is used as the f_z component of the forcing function, while the f_x component is set to zero. The displacement solutions for the elastic wave equations are computed at an array of receiver locations at z = 0.8 m, x = [-1 m, 1 m] in the x-z coordinate system [12]. They are subsequently used to obtain analytical results for the applied forcing function. Results comparing these with the corresponding FDTD simulations are presented in [7].

III. Simulation of Pneumothorax

As described earlier in Section I, a pneumothorax is basically an air pocket trapped in the pleural space between the lung and the chest wall. The condition is thus modeled by introducing a region at the exterior edge of the lung that has material properties of air, as shown in Fig. 2. In order to study the effect of the size of the air-pocket on the chest signals, sizes varying from 1.7 cm to 5 cm was introduced, size being defined as the maximum extent of the air cavity.

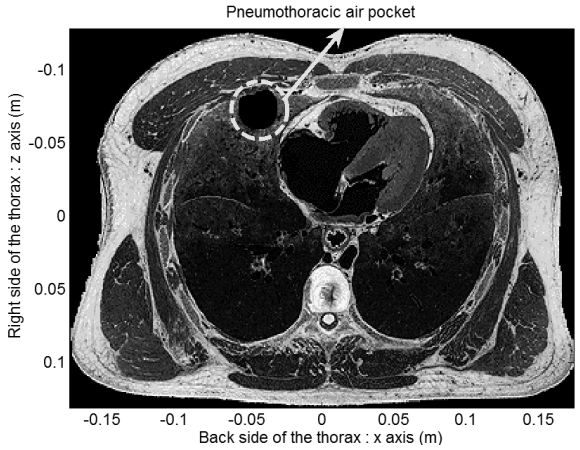

Fig. 2. Anatomical simulation of a pneumothoracic air cavity

To model the sound wave propagation in the thoracic cavity, we first discretize the transverse cross-sectional slice image of the thorax. The rectangular domain of L_x X L_z = 35 cm X 25 cm enclosing the thorax is discretized into N_x X N_z cells using the grid size as determined in (2). PML layers, 15 cm thick, surrounded this rectangular domain on each side. The time step was chosen to be 0.8 times the Courant limit as defined in (3).

The 2D FDTD codes were used to calculate the velocity and stress components at an array of sensor locations placed all around the torso. Subsequently, the mean pressure, p was computed using the normal stress components as follows:

$$p = -(T_{xx} + T_{zz})/2 \tag{5}$$

The simulations used the following parameter values:

$$\begin{aligned}
&\text{Grid size} : \Delta x = \Delta z = 1mm \\
&\text{Dimensions} : N_x = 350,\ N_z = 250, \\
&\qquad PML_{width} = 150\ layers \\
&\text{Time step} : \Delta t = 0.15\mu\,\text{sec} \\
&\text{Source function} : f_0 = 300\,Hz,\ A = 10^6 \\
&\text{Sampling frequency} : F_S = 8000\,Hz \\
&\gamma \text{ values} : \gamma_{xx} = \gamma_{zz} = \gamma_{xz} = 300\ \forall x, z
\end{aligned} \tag{6}$$

IV. Results

Using the simulated pressure waveforms at the sensor locations around the torso and the source forcing function, the source-to-sensor transfer functions (TF) were computed for each pneumothorax simulation. For ease of analysis, we consider only one of the key sensor locations on the front surface of the chest, indicated by a white cross in the top row of images of Fig. 3. The source location is indicated by the white circle in the images. These images represent the various pneumothorax conditions simulated with increasing degree of severity going from left to right. The bottom row plots in Fig. 3 represent the amplitudes of the source-to-sensor pressure TFs for the corresponding pneumothorax condition. The left most image and TF plot corresponds to a normal thorax. The maximum amplitude of the TF obtained for the normal thorax is used as the scaling factor for all the plots in this figure and subsequent figures.

In order to further study and compare these TFs, Fig. 4 plots these on one common axis. We notice that at frequencies around 50-100 Hz there isn't any significant difference in the amplitudes of the TFs. However, the frequency range of 350-475 Hz shows a distinct trend of decreasing amplitudes with increasing degree of severity of pneumothorax. Fig. 5 considers the amplitudes of the difference transfer functions (DTF), computed as:

$$DTF = TF(Pneumothorax) - TF(Normal) \tag{7}$$

The plot shows that the deviation of the TF from the normal case is the largest for the pneumothorax with the largest air cavity (5 cm, in this case), and shows a clear trend across all the cavity sizes. More importantly, this deviation is enhanced in the 350-475 Hz frequency range, thereby providing some additional insight into possible diagnostic utility of chest signals measured in this frequency range.

Similar results may be obtained from other sensor sites too. As one would expect, sites located significantly distant from the air cavity do not show such prominent deviation. Thus, by combining information from various sensor sites, one could devise a multi-sensor noninvasive auscultatory system for diagnosis of pneumothorax conditions.

V. Conclusions

A 2D numerical FDTD viscoelastic model has been used to study the lung sound propagation in the human thoracic cavity under pneumothorax conditions by considering the exact geometry of the torso along with the precise material properties of each of the tissues. The model thus provides a

convenient test-bed to investigate the possibility of using an array of noninvasive acoustic sensors for diagnosing pneumothorax and estimating the extent of severity of the disease. Future efforts would be directed towards developing a 3D model of the torso that may provide a more accurate representation of the thoracic sounds. Studies pertaining to effects of the location of the cavity in the thorax would be considered. Furthermore, the models would be used to design and evaluate various inversion schemes that can be used to estimate the location and size of the air cavity.

REFERENCES

[1] H. A. Mansy, T. J. Royston, R. A. Balk, and R. H. Sandler, "Pneumothorax detection using pulmonary acoustic transmission measurements," *Med. Biol. Eng. Comput.,* vol. 40, pp. 520–525, 2002.

[2] D. Lichenstein, G. Meziere, P. Biderman, and A. Gepner, "The 'lung point': an ultrasound sign specific to pneumothorax," *Intensive Care Med.,* vol. 29, pp. 1434-1440, 2000.

[3] H. A. Mansy, T. J. Royston, R. A. Balk, and R. H. Sandler, "Pneumothorax detection using computerised analysis of breath sounds," *Med. Biol. Eng. Comput.,* vol. 40, pp. 526–532, 2002.

[4] I. V. Vovk, V. T. Grinchenko and V. N. Oliynik, "Modeling the acoustic properties of the chest and measuring breath sounds," *Acoust. Phys.*, vol. 41, pp. 667-676, 1995.

[5] C. Narasimhana, R. Wardb, K. L. Kruseb, M. Guddatic, and G. Mahinthakumar, "A high resolution computer model for sound propagation in the human thorax based on the Visible Human data set," *Computers in Biology and Med.*, vol. 34, pp. 177-192, 2004.

[6] S. Acikgoz, M. B. Ozer, T. J. Royston, H. A. Mansy, and R. H. Sandler, "Experimental and computational models for simulating sound propagation within the lungs," *J Vib Acoust.*, vol. 130, 021010, 2008.

[7] S. Ramakrishnan, S. Udpa, and L. Udpa, "A numerical model simulating sound propagation in human thorax (Accepted for publication)," in *2009 Proc. IEEE Int. Symp. Biomedical Imaging*, to be published.

[8] A Guided Tour of the Visible Human, MAD Scientist Network, Washington University Medical School, 1996. Available: www.madsci.org/~lynn/VH/tour.html

[9] F. H. Drossaert and A. Giannopoulos, "A non-split complex frequency shifted PML based on recursive integration for FDTD modeling of elastic waves," *Geophysics*, vol. 72, pp. T9-17, 2007.

[10] C. Schroder and W. Scott, Jr., "On the stability of the FDTD algorithm for elastic media at a material interface," *IEEE Trans. Geosci. Remote Sensing*, vol. 40, pp. 474-481, 2002.

[11] J. Virieux, "P-SV wave propagation in heterogeneous media: velocity–stress finite-difference method," *Geophysics*, vol. 51, pp. 889–901, 1986.

[12] G. Eason, J. Fulton, and I. N. Sneddon, "The generation of waves in an infinite elastic solid by variable body forces," *Phil. Trans. Royal Soc. London (A)*, vol. 248, pp. 575-607, 1956.

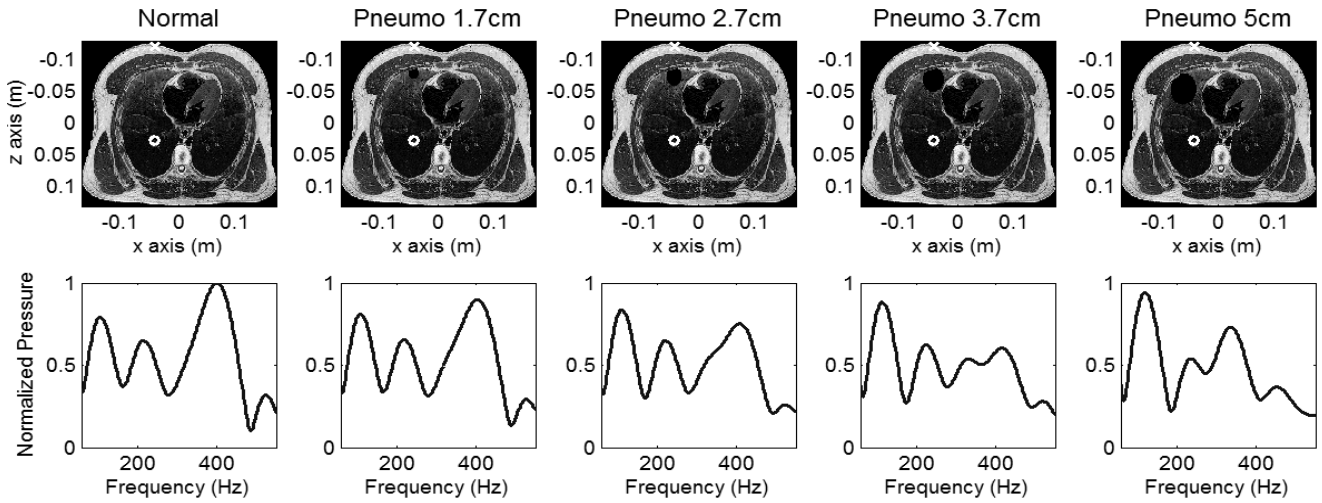

Fig. 3. Top row of images show the cross-sectional slice of the thorax for varying sizes of the pneumothoracic air pocket in the lung. The bottom row of plots represent the corresponding amplitude of the source(o)-to-sensor(x) transfer functions.

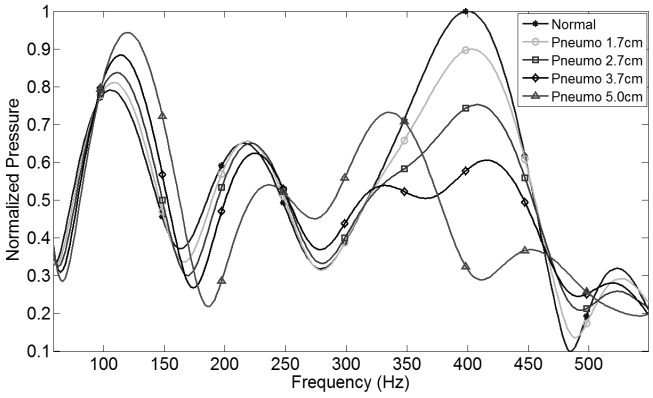

Fig. 4. Comparison of the amplitudes of the source-to-sensor transfer functions corresponding to varying sizes of the pneumothoracic air pocket.

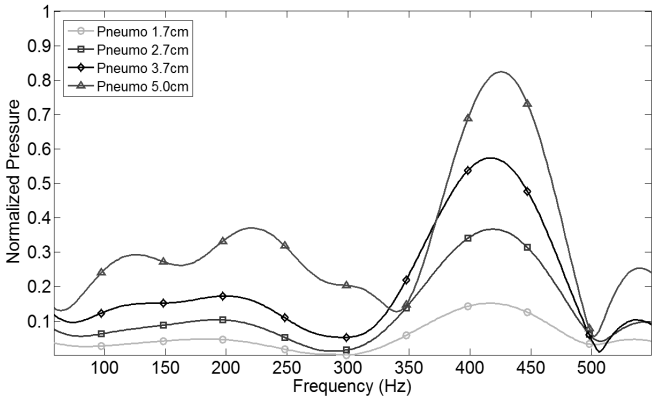

Fig. 5. Comparison of amplitudes of difference of the transfer functions of varying degrees of pneumothoracic severity and that of a normal thorax.